https://doi.org/10.5194/nhess-2020-209
Preprint. Discussion started: 20 July 2020

Natural Hazards and Earth System Sciences
Discussions

Laboratory study of non-linear wave-wave interactions of extreme focused waves in the nearshore zone

Iskander Abroug [1, 2], Nizar Abcha [1], Armelle Jarno [2], François Marin [2]

[1] Normandie Université, UNICAEN, UNIROUEN, CNRS, UMR 6143 M2C, 14000 Caen, France.
[2] Normandie Université, UNILEHAVRE, CNRS, UMR 6294 LOMC, 76600 Le Havre, France.

Correspondence to: Iskander Abroug (iskander.abroug@unicaen.fr)

Abstract. Extreme waves play a crucial role in marine inundation hazards and coastal erosion. In this article, we experimentally study nonlinear wave-wave interactions of large amplitude focused wave groups propagating in a two-dimensional wave flume over a mild slope ($\beta = 1{:}25$). The influence of the frequency spectrum and the steepness on the nonlinear interactions of focused waves are examined. The generated wave trains correspond to Pierson-Moskowitz and JONSWAP ($\gamma = 3.3$ or $\gamma = 7$) spectra. Subsequently, we experimentally approach this problem by the use of a bispectral analysis applied on short time series, via the wavelet-based bicoherence parameter, which identifies and quantifies the phase coupling resulting from non-resonant or bound triad interactions with the peak frequency. The bispectral analysis shows that the number of frequency components participating in the focusing process and the resulting quadratic phase coupling increase gradually and approaches 1 just prior to breaking, accordingly with the spectrum broadening and the energy increase in high frequency components. Downstream breaking, the values of phase coupling between the peak frequency and its harmonics decrease drastically and the bicoherence spectrum becomes less structured.

1 Introduction

Extreme wave propagation is a highly nonlinear process observed in both open seas and coastal regions. The main physical mechanisms which may lead to an extreme wave event are illustrated in Kharif and Pelinovsky, 2003; Kharif et al., 2009; Didenkulova et al., 2010; Onorato et al., 2013. Extreme waves may occur in deep or shallow water, in energetic storm sea state or previously calm sea state. In our opinion, spatio-temporal wave focusing is one of the most important mechanisms in the extreme wave formation for shallow and deep water (Kharif and Pelinovsky, 2003). The spatio-temporal wave focusing is a classical mechanism giving rise to an important wave energy concentration in a small region. If the wave height of the focusing group exceeds 2.2 times its significant wave height, it can be defined as a rogue or freak wave (Dysthe et al., 2008). For this reason, spatio-temporal wave focusing is often employed in laboratory wave flumes with a wide variation of water depth (Merkoune et al., 2013), spectrum type (Tian et al., 2011; Xu et al., 2019; Abroug et al., 2019; 2020) and wavelength to depth ratio, in order to better understand the generation process, the dynamic behavior and the hydrodynamic loads on ocean structures in extreme sea conditions.

https://doi.org/10.5194/nhess-2020-209
Preprint. Discussion started: 20 July 2020


Natural Hazards and Earth System Sciences Discussions

Over the past years, several studies have attempted to quantify the spatial evolution of spectral energy of unidirectional wave groups in experimental wave flumes using a classic Fourier analysis (Tian et al., 2011; Liang et al., 2017; Abroug et al., 2020). The frequency spectrum only gives the energy distribution in the spectral domain; however, the quadratic phase coupling among different wave frequencies is unknown. Consequently, higher-order spectrum techniques should be used in understanding nonlinearity. A powerful tool to investigate the highly nonlinear process is the wavelet-based bispectral technique, which has been used in several works to study the non-linear interactions and quadratic phase coupling between wave components (Guohai et al., 2008; Ma et al., 2010). The need to detect and quantify second order non-linear interactions can be found in many disciplines, such as, geophysics (Grinsted et al., 2004), plasma physics (Milligan et al., 1995), fault diagnosis (Li et al., 2014), health-related areas, neuroscience (Bai et al., 2017) and wave analysis (Eldeberky, 1996; Eldeberky and Madsen, 1999; Young et al., 1996; Young and Eldeberky, 1998; Becq-Girard et al., 1999; Huseni and Balaji, 2017; Zhang et al., 2019). In wave analysis, the propagation of wave trains in the nearshore zone has an exceptionally high spectral and temporal resolution.

The majority of previous works concerning the spatial evolution of group focused waves in numerical and experimental wave flumes have shown that spatio-temporal focusing leads to a shape and elevation of a wave crest at focus that cannot be estimated accurately by linear or 2nd order wave theory. This is due to high order nonlinearities, called the bound (harmonics) and resonant nonlinearities (Vyzikas et al., 2018). On the one hand, bound nonlinearities are the result of non-linear harmonics that are phase-locked to the wave train and contribute in the sharpening of free surface elevation. On the other hand, resonant interactions contribute in the energy redistribution among different frequency components (Vyzikas et al., 2018). It is important to mention here that resonant interactions are not easily achieved in unidirectional wave train propagation since the resonant conditions cannot not be satisfied in a small area. Therefore, we investigate specifically the role of bound waves generated by non-resonant three-wave coupling.

Over the past few decades, various experimental studies have investigated the spatial evolution of non-linear coupling between wave components. Guohai et al., 2008 studied the spatial evolution of non-linear interactions among different wave components in the shoaling and de-shoaling zones by carrying out two random waves derived from JONSWAP spectra with varying waves heights and peak waves periods. They showed that the quadratic phase coupling increases rapidly in the shoaling region and achieves its highest level prior to wave breaking. Ma et al., 2010 studied experimentally JONSWAP wave trains propagating in intermediate water depth. Recently, nonlinear transformation of unidirectional irregular waves propagating over a complex bathymetry ($1.06 < k_p h < 2.2$; where k_p is the peak wavenumber and h denotes the water depth) was performed in Zhang et al., 2019, who studied the triad wave-wave non-linear interactions in the case of long records of JONSWAP irregular waves (1200 T_p, where T_P is the peak period) using a Fourier-based bispectral analysis. They found that the phase coupling is strong near the end of the slope, where second and third harmonics become more important. They also noticed the appearance of low-frequency waves generated by the difference interactions during wave propagation. We must note here that the main difference between wavelet-based bicoherence and Fourier-based bicoherence is the number of degrees of freedom (Guohai et

https://doi.org/10.5194/nhess-2020-209
Preprint. Discussion started: 20 July 2020


Natural Hazards and Earth System Sciences Discussions

al., 2008). Wavelet-based bicoherence is a suitable tool to capture quadratic phase couplings occurring in relatively short data sequences, and can be used to analyse data collected in laboratory flumes (Elsayed, 2006).

Most of the above-mentioned studies were performed in random wave conditions based on JONSWAP spectra. To the author's knowledge, few studies have attempted to quantify the degree of phase coupling resulting from the propagation of realistic spectrum focused waves in the inner surf zone using wavelet-based bicoherence. Experiments are performed on numerous Pierson-Moskowitz and JONSWAP wave trains propagating from a constant intermediate water depth to shoaling and breaking regions.

The paper is outlined as follows. Section 2 describes the experimental procedure and the studied wave train parameters. In section 3, a short formal description of wavelet analysis and wavelet-based bicoherence is provided. The spatial evolution of wavelet-based bicoherence is discussed in section 4. The conclusions and perspectives of this study are given in section 5.

2 Experimental setup and wave train parameters

The following is a brief consideration of present wave trains generation; more details of the experiments can be found in Abroug et al., 2020. The experiments were conducted in a two-dimensional wave flume of the Morphodynamique Continentale et Côtière laboratory at Caen University, France. The flume is 22 m long, 0.8 wide and the water depth is h_0 = 0.3 m (Fig. 1). In this study, the relative water depth $k_p h_0 < 1.363$ is verified, which means that the modulation instability effect can be neglected (Janssen et al., 2007; Fedele et al., 2019). An Edinburgh Designs Ltd piston type wavemaker is located at one end of the flume to implement wave trains using linear wave generation signal. Wave trains are generated with almost no reflection at the end of the flume, since free surface elevations are measured before reflected waves travel back. Thus, the occurrence of resonant interactions potentially driven by reflected waves is limited and we only focus on bound waves.

The data used in this work are issued from Abroug et al., 2020. The present study relates to seven wave trains derived from the averaged JONSWAP spectra (i.e. with peak factor γ = 3.3 or 7) or Pierson-Moskowitz spectra with varied peak wave periods f_p and wave steepnesses S_0 (i.e. non-linearity). For each wave train, a large number of wave signals were recorded along the flume to accurately follow the wave evolution in space. The surface elevation is measured by two aligned wave gauges located from the longitudinal coordinate x_{min} = 4 m to x_{max} = 14 m, where x = 0 represents the mean position of the wavemaker. The positions of these wave gauges are indicated in Fig. 1. The sampling rate is 50Hz and each record duration is ΔT = 35 s with a sample interval of 0.02 s. The fast Fourier transform (FFT) was applied to each signal, resulting in 1750 frequency components over the range [0, $3f_p$] and with a spectral resolution Δf = 0.023 Hz. The distance from the wave maker for the focusing point was set to 12 m from the wave maker.

https://doi.org/10.5194/nhess-2020-209
Preprint. Discussion started: 20 July 2020

Natural Hazards and Earth System Sciences
Discussions

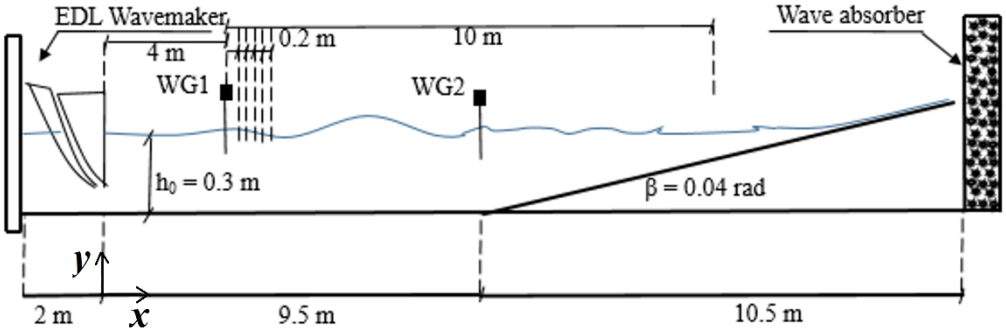

Figure 1: Schematic experimental setup, WG1 and WG2 denote wave gauge n°1 and wave gauge n°2 respectively.

The free surface elevation of a wave train at a distance x from the wavemaker can be written using linear wave theory:

$$\eta(x,t) = \sum_{i=1}^{N} a_i \cos(k_i x - \omega_i t - \Phi_i) \quad (1)$$

where ω_i is the frequency of each wave component, where i varies from 1 to N (number of waves), k_i the wave number, a_i the amplitude and Φ the phase of the wave group within its envelope at the focus position. Based on Eq. (1), the varied parameters during these experiments were the spectrum type and the wave steepness S_0. The peak frequency parameter was chosen in order to have a relative depth $k_p h_0$ varying between 0.79 and 0.92 (Deep side in Table 1). Deep and shallow sides in Table 1 represent respectively the flat bottom depth (4 m < x < 9.5 m) and the shallowest studied depth (x = 14 m). Five of the studied wave trains have more than one breaking and breaking locations x_b are indicated as bracketed intervals in Table 1.

Table 1. Wave trains key parameters

Test	f_p (Hz)	S_0	Spectrum type	x_b (m)	$k_p h_0$	$k_p h$
					Deep Side	Shallow Side
1	0.70	0.19	Gaussian	[11.85;12.55]	0.84	0.34
2	0.66	0.14	Pierson-Moskowitz	12.9	0.79	0.31
3	0.66	0.28	Pierson-Moskowitz	[11.09;11.82]	0.79	0.31
4	0.75	0.25	JONSWAP (γ=3.3)	[12.13;12.81]	0.92	0.37
5	0.75	0.38	JONSWAP (γ=3.3)	[10.5;11.61]	0.92	0.37
6	0.75	0.11	JONSWAP (γ=7)	13.5	0.92	0.37
7	0.75	0.23	JONSWAP (γ=7)	[12.07;12.69]	0.92	0.37

https://doi.org/10.5194/nhess-2020-209
Preprint. Discussion started: 20 July 2020


Natural Hazards and Earth System Sciences
Discussions

3 Wavelet-based analysis

The free surface elevation of each wave train was studied through the bispectral analysis applied on short time series, via the wavelet-based bicoherence tool. Detailed specifications of the wavelet-based bicoherence are outlined in Van Milligen et al., 1995 and a brief introduction of this technique is given below. The continuous wavelet transform WT (a,τ) of a time series $f(t)$ is calculated as:

$$WT(a,\tau) = \int_{-\infty}^{+\infty} f(t)\psi_{a,\tau}^{*}\, dt \quad (2)$$

where the asterisk denotes the complex conjugate and $\psi_{a,\tau}$ represents the mother wavelet function dilated by a factor τ and scaled by a factor a, $a > 0$. The latter parameter can be interpreted as the frequency inverse, i.e. $f = 1/a$. The wavelet transform can be interpreted as a series of bandpass filter of the time series with a mother wavelet function. We have chosen the Morlet wavelet as a mother wavelet function since it furnishes information about phase and amplitude, and it is appropriate for capturing coherence between different harmonic components. The Morlet wavelet can be considered as a modulated Gaussian waveform and is defined as follows:

$$\psi(t) = \pi^{-1/4} e^{-\frac{t^2}{2}} e^{(i\omega_0 t)} \quad (3)$$

where ω_0 denotes the dimensionless frequency and t is the dimensionless time. The Morlet wavelet with $\omega_0 = 6$ is a good choice, since it ensures a good balance between time and frequency localisation (Grinsted et al., 2004; Guohai et al., 2008). For the Morlet wavelet the scale a is almost equal to the Fourier period T ($T = 1.03\ a$). From a practical point of view, the scales a can be expressed as fractional powers of two (Guohai et al., 2008; Torrence and Compo, 1998):

$$a_i = a_0 2^{i\delta}, i = 0,1,2,\ldots,M \quad (4)$$

$$M = \frac{1}{\delta} log_2\left(\frac{N\Delta t}{a_0}\right) \quad (5)$$

where a_0 is the smallest resolvable scale, M represents the largest scale and δ denotes the scale factor. The a_0 parameter should be chosen equal to $2\times\Delta t$ (Torrence and compo, 1998; Guohai et al., 2008). $N = 1750$ and $\Delta t = 0.02$ s represent respectively the number of points in $f(t)$ and the sampling time. The scale factor δ should be sufficiently small to provide high resolution and satisfactory sampling in scale. Moreover, a scale factor $\delta = 0.5$ is the largest value that gives adequate sampling in the case of the Morlet wavelet (Guohai et al., 2008). It is for that reason that we opted for a scale factor $\delta = 0.02$, giving a total of 395 scales ranging from 0.04 up to 11.83 for respectively high and low frequency. The wavelet-based bispectrum (Eq. (6))

https://doi.org/10.5194/nhess-2020-209
Preprint. Discussion started: 20 July 2020


Natural Hazards and Earth System Sciences
Discussions

determines quantitatively during ΔT = 35 s the phase coupling that occurs between f_1, f_2 and f_3 where the latter parameters must satisfy Eq. (7). Quadratic non-linear coupling occurs between f_1 and f_2, generating a third component at the sum frequency f_3. The bispectrum (Eq. (6)), which is the double Fourier transform of the third-order moment, measures the extent of phase coherence due to the non-linear triad interaction between three waves that satisfy the frequency and phases matching criteria (Eq. (7) and (8)). The estimation of wavelet-based bispectrum in the bifrequency plan can be based on its values in the interval $\psi : \{f_1 > f_2 > 0, f_1+f_2 = f_s = 25$ Hz (Nyquist sampling frequency)$\}$.

$$B(a_1, a_2) = \int WT_x(f_1, \tau)\, WT_x(f_2, \tau) WT_x^*(f_3, \tau) d\tau \quad (6)$$

$$f_3 = f_1 + f_2 \quad (7)$$

$$\varphi_3 = \varphi_1 + \varphi_2 \quad (8)$$

The wavelet-based bicoherence (Eq. (9)), which can be defined as the normalised wavelet bispectrum, is used in practise to measure the degree of phase coupling (Larsen et al., 2001) and is bounded by 0 and 1 by the Schwarz inequality. A value close to unity reveals a maximum amount of coupling and a value close to zero corresponds to a random phase relation.

$$b^2(a_1, a_2) = \frac{|B(a_1,a_2)|^2}{\left[\int_{t=0}^{t=35} |WT_x(a_1,\tau) WT_x(a_2,\tau)|^2 d\tau\right] \int_{t=0}^{t=35} |WT_x(a_3,\tau)|^2 d\tau} \quad (9)$$

Figure 2 exhibits a simple illustration of the wavelet-based bicoherence of a narrow-banded Gaussian wave train (Test 1) recorded at x = 4 m from the wavemaker. The shading indicates the strength of non-linear coupling; dark red ($b^2(f_1, f_2) = 1$) being totally coupled and dark blue ($b^2(f_1, f_2) = 0$) completely uncoupled. The degree of phase coupling is represented by the colorbar indicating the sum interactions between two frequencies. In this manner, a visualisation of the non-linear activity across the wave train propagation is realisable, detecting the frequency components that contribute the most to the non-linear activity. The two frequencies f_1 and f_2 are normalised by the peak frequency f_p. Red ($b^2(f_p, f_p)$) and yellow peaks represent the phase coupling of the primary frequency component with its harmonic. In general, a non-null bicoherence $b^2(f_1,f_2) > 0$ means that the $f_3 = f_1+f_2$ component gains energy from the f_1 and f_2 components.

https://doi.org/10.5194/nhess-2020-209
Preprint. Discussion started: 20 July 2020

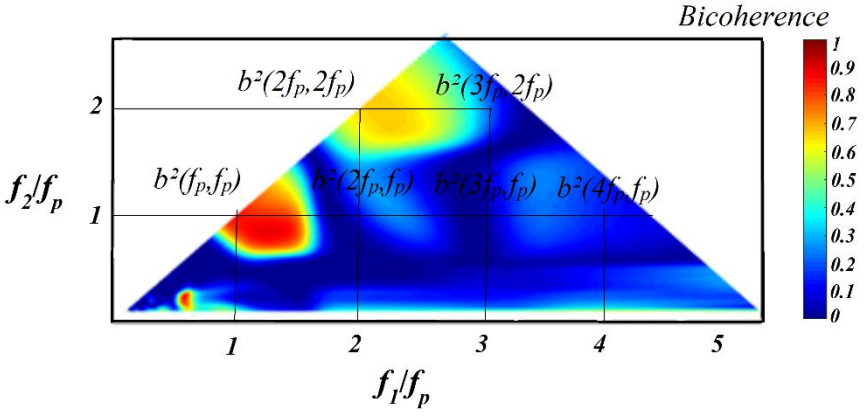

Figure 2: The wavelet-based bicoherence of a narrow-banded Gaussian wave train (Test 1) at x = 4 m.

4 Results and discussions

Figure 3 shows three sets of time series of three wave trains with approximately the same steepness S_0 and derived from Pierson-Moskowitz (Test 3), JONSWAP (γ = 3.3) (Test 4) and JONSWAP (γ = 7) (Test 7) spectra at eight different locations along the flume. This preliminary figure shows surface elevation time histories including the first measurement (x = 4 m), the propagation along the flat bottom, the shoaling and the breaking of the focused wave group. It should be noted here that the seven studied wave trains are crest-focused wave groups (Φ = 0).

Figure 4 shows, in a log scale, the spatial evolution of the Fourier spectra of the same three wave trains (Tests 3, 4 and 7). A spatial downshift of the spectral peak (Cases 4 and 7), a steepening of the low frequency side and a widening of the high frequency side are illustrated. These spectral variations, identified and quantified in Abroug et al., 2020, concern high and low frequency components. The shift of energy is essentially due to non-linear wave-wave interactions between wave components during the focalisation process. However, we do not distinguish which wave components are involved in the wave-wave interactions and the wave modes that undergo the strongest non-linear interactions. Consequently, the wavelet bicoherence tool is used herein to provide information about the non-linear wave interactions that are not easily obtained from the Fourier analysis which was used in Abroug et al., 2020.

https://doi.org/10.5194/nhess-2020-209
Preprint. Discussion started: 20 July 2020

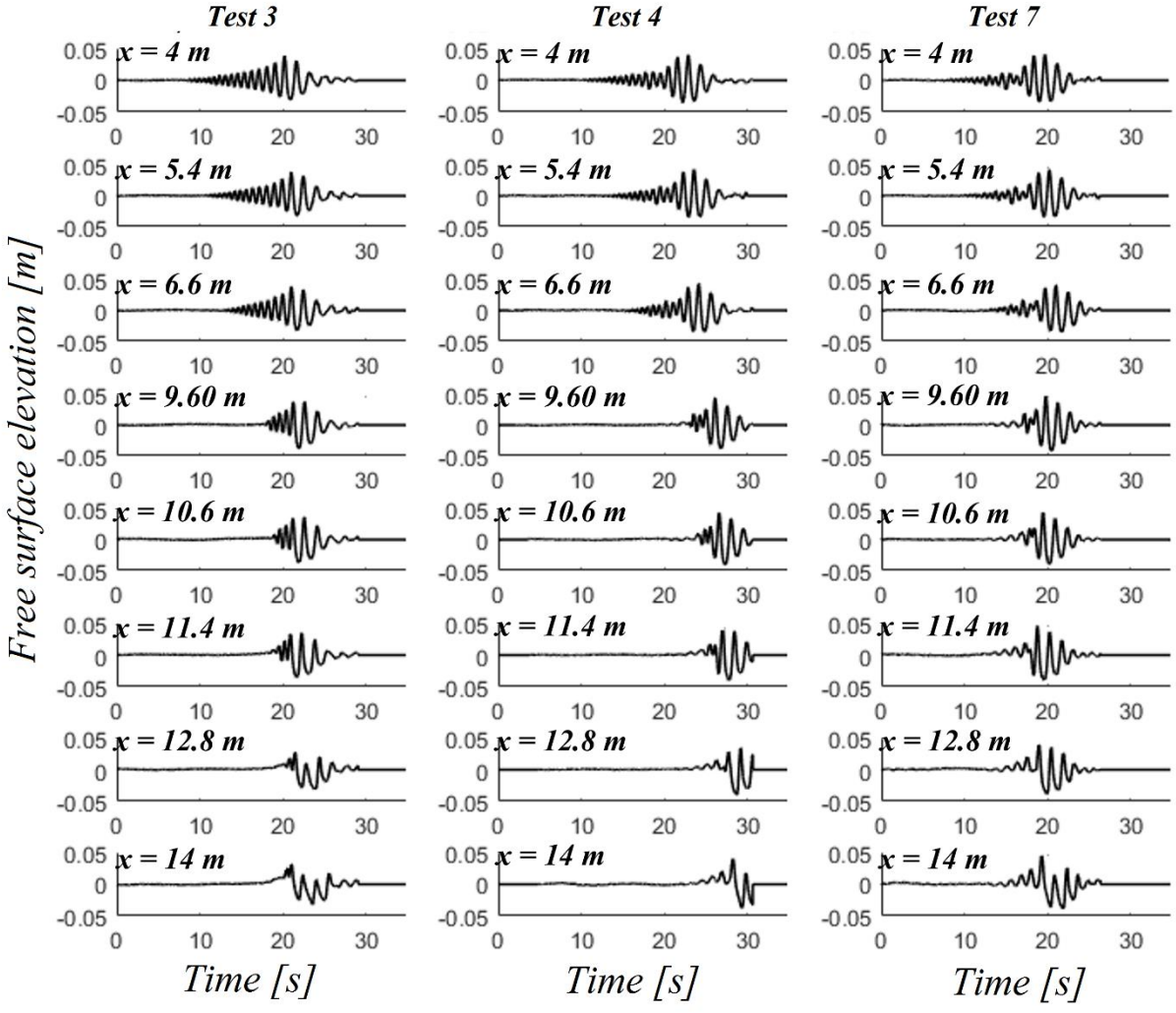

Figure 3: Three sets of time series of Pierson-Moskowitz (Test 3), JONSWAP (γ = 3.3) (Test 4) and JONSWAP (γ = 3.3) (Test 7) wave trains.

Figure 5 presents the spatial evolution of the wavelet-based bicoherence of a Pierson-Moskowitz wave train (Test 3) along the flat bottom. This figure shows that wave-wave interactions between different modes are weak on flat bottom (4 m < x < 9.5 m; $k_p h_0$ = 0.79) and few frequency components participate in the focusing process. In the intermediate water depth region (4 m < x < 9.5 m), the sea state is almost Gaussian, and for that reason non-linear wave-wave interactions are relatively moderate. For example, $b^2(f_p, f_p)$ = 0.1 and $b^2(f_p, 3f_p)$ = 0.065 at x = 4 m, indicate respectively a weak self-self wave interaction at the peak frequency f_p coupled with the energy at $2f_p$ and a very weak wave interaction at f_p coupled with the energy at $4f_p$ (Fig. 5a). A significant bicoherence magnitude band ranging from $0.5f_p$ to f_p is observed, i.e. $b^2(0.5f_p - f_p, 0.5f_p - f_p)$, which indicates an energy transfer from low frequency components to the spectral peak. This partially explains the spatial evolution of the spectrum, namely the increase of energy in the peak region, which is potentially due to a compensating mechanism of

https://doi.org/10.5194/nhess-2020-209
Preprint. Discussion started: 20 July 2020

Natural Hazards and Earth System Sciences
Discussions

the energy dissipation in the transfer region, i.e. the region between the spectral peak and high frequency regions, (Abroug et al., 2020; Liang et al., 2017). Note that the magnitude of the bicoherence is consistent with the fact that spectrum shape does not vary substantially along the flat bottom (4 m < x < 9.5 m) (Fig. 4).

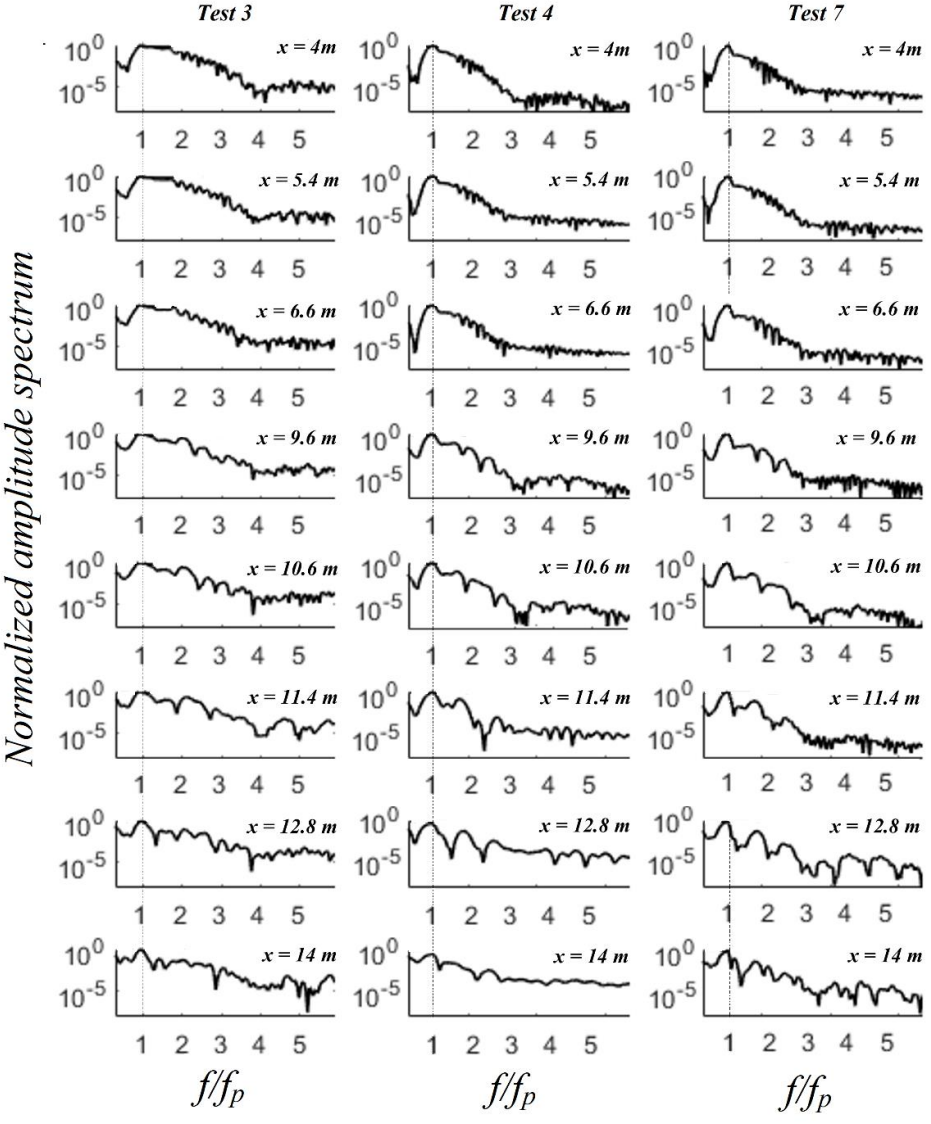

Figure 4 : Spatial evolution of normalised amplitude spectra in a log scale for Tests 3, 4 and 7.

As the wave packet approaches the toe of the beach (x ~ 9.5 m), more and more wave components are involved in the quadratic phase coupling and the bicoherence values increase progressively. For x = 9.6 m, just a little over the toe of the slope, the bicoherence magnitude among primary components increases slightly, i.e. $b^2(f_p, f_p) = 0.24$ and $b^2(3f_p, f_p) = 0.15$, which is consistent with the small energy increase in the high frequency region (Abroug et al., 2020).

https://doi.org/10.5194/nhess-2020-209
Preprint. Discussion started: 20 July 2020

Natural Hazards and Earth System Sciences
Discussions

As the wave train propagates in the shallower region ($9.5\ \text{m} < x < x_b \in [11.09; 11.82]$), the non-linear phase coupling is seen to increase rapidly (Fig. 6a). The quadratic phase coupling within f_p increases considerably at shallower regions compared to deeper regions. Wave energy transfers increase in high frequency region and as a result, the spectrum broadens. In the vicinity of the breaking location ($x_b \in [11.09; 11.82]$), the non-linear coupling spreads over most of the wave components. The increase of the second and third harmonic is clearly noticeable in Fig. 6b. The wavelet-based bicoherence for approximately all frequency pairs is higher than 0.13, revealing that the non-linear phase coupling reaches its maximum level, which means that nearly all of the higher harmonics wave components are involved in the propagation process.

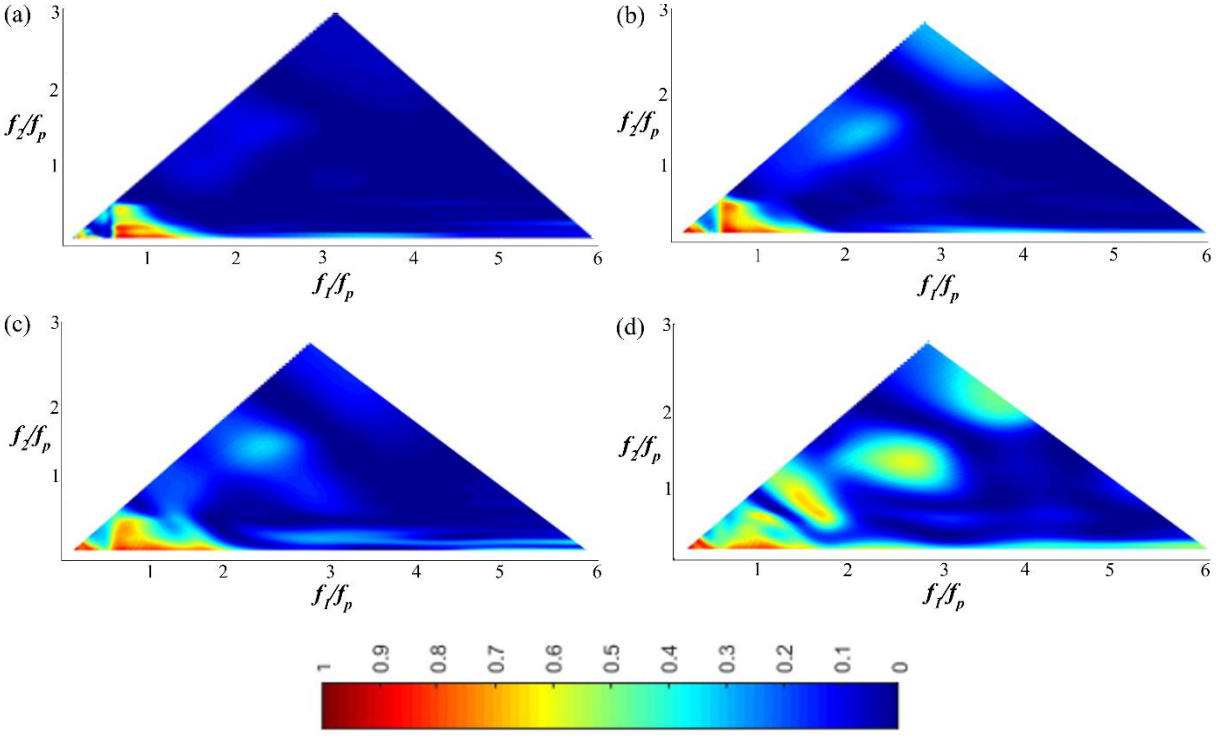

Figure 5 : The wavelet-based bicoherence spatial evolution on the flat bottom for a Pierson-Moskowitz wave train (Test 3). (a): x = 4 m; (b): x = 5 m; (c): x = 8 m; (d): x = 9.6 m.

Downstream the breaking location ($x > x_b \in [11.09; 11.82]$), the quadratic phase coupling among frequency components decreases drastically and the bicoherence becomes less structured (Fig. 6d). This result is consistent with the decreasing trend of energy in higher frequency components downstream the breaking location (Tian et al., 2011; Abroug et al., 2020).

https://doi.org/10.5194/nhess-2020-209
Preprint. Discussion started: 20 July 2020

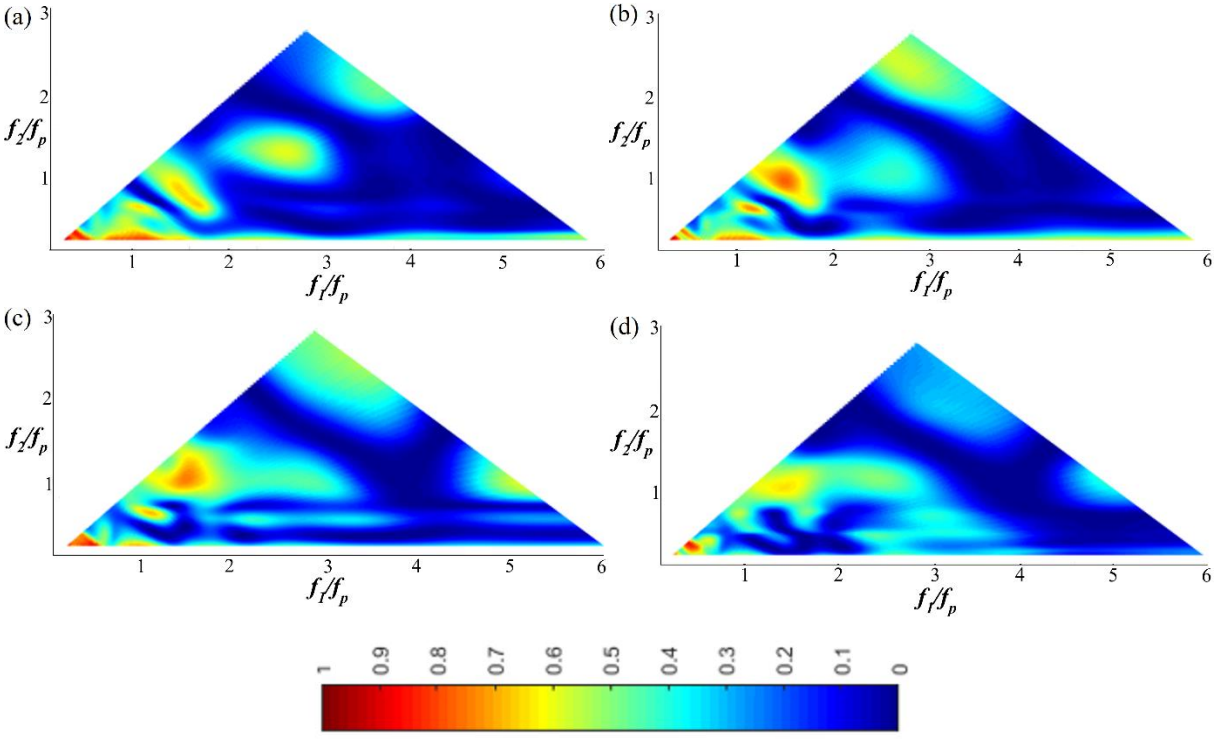

Figure 6 : The wavelet-based bicoherence spatial evolution on the sloping bottom for a Pierson-Moskowitz wave train (Test 3). (a): x = 11 m; (b): x = 12 m; (c): x = 13 m; (d): x = 13.8 m.

In fig. 7 and 8, a JONSWAP (γ = 3.3) wave train (Test 5) is chosen to illustrate the spatial evolution of the wavelet-based bicoherence of a narrower wave train propagating over the flat and the sloping bottom. Wave-wave interactions evolve qualitatively in the same way compared to the case of Pierson-Moskowitz. Fig. 7a (x = 4 m) shows that the two dominant phase coupling peaks appear at the bifrequencies (f_p, f_p) and (0.5f_p, 0 - 0.5f_p), which illustrates that the quadratic non-linear interactions only occur between the peak and low-frequency modes. Note that no other peak was found to be significant. As the wave train propagates over the shallower region (x > 9.5 m), new phase couplings appear at the bifrequencies (2f_p, f_p), (3f_p, f_p) and (2f_p, 3f_p) (Fig. 8). This finding illustrates that quadratic non-linear interactions between the peak frequency, the first harmonic, the second harmonic and third harmonics result from the gradual broadening of the spectrum. It is an accordance with previous studies demonstrating that energy is mainly transferred to high frequencies during the shoaling process (Tian et al., 2011; Liang et al., 2017; Abroug et al., 2020). For this wave train (Test 5), the wavelet-based bicoherence reaches its maximum shortly after the breaking at x = 12 m. For example, $b^2(f_p, f_p) = 0.7$, $b^2(2f_p, f_p) = 0.53$ and $b^2(2f_p, 2f_p) = 0.16$. Triad interactions lead to skewed wave profiles and can characterize the near-breaking conditions (Fig. 3 for x > 10.6 m).

https://doi.org/10.5194/nhess-2020-209
Preprint. Discussion started: 20 July 2020

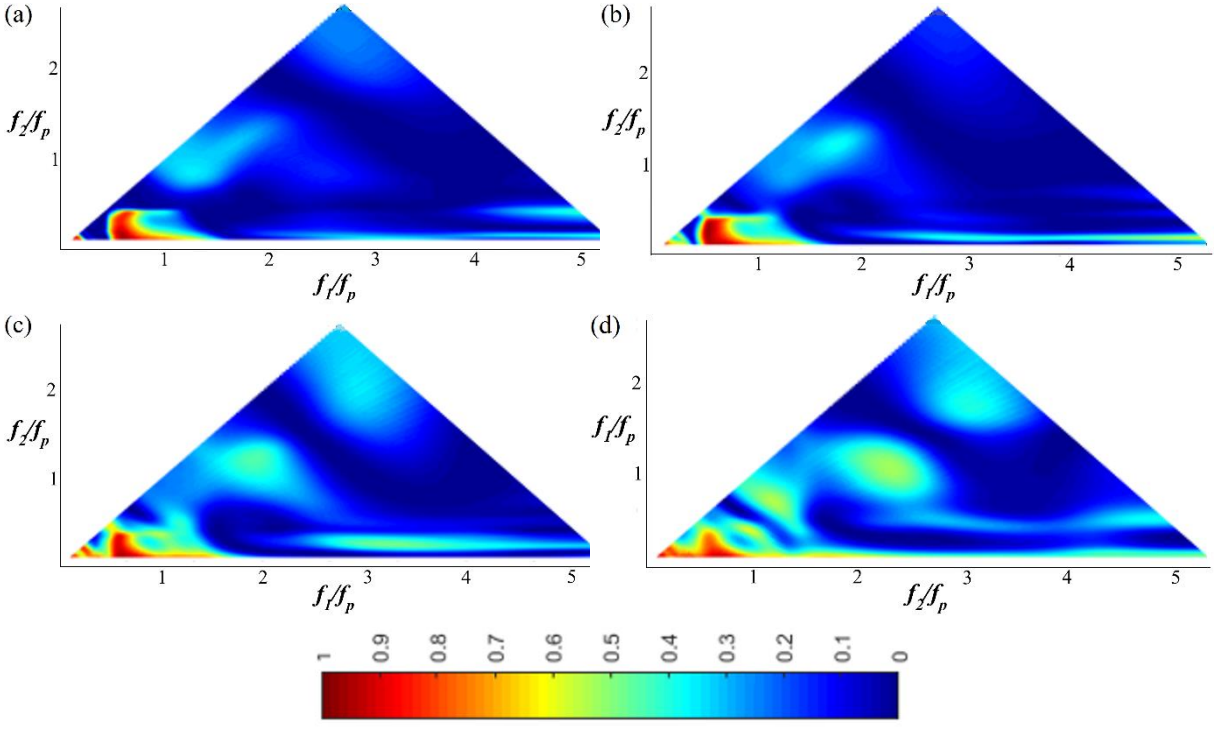

Figure 7: The wavelet-based bicoherence spatial evolution on the flat bottom for JONSWAP ($\gamma = 3.3$) wave train (Test 5). (a): $x = 4$ m; (b): $x = 6$ m; (c): $x = 8$ m; (d): $x = 9.6$.

Beyond the breaking location ($x > x_b \in [10.5;11.61]$), the bicoherence decreases sharply and becomes less structured. For example $b^2(f_p, f_p) = 0.52$, $b^2(2f_p, f_p) = 0.31$ and $b^2(2f_p, 2f_p) = 0.004$ at $x = 13.6$ m, i.e. $h = 0.13$ m. This pattern is qualitatively similar to that obtained in the case of a Pierson-Moskowitz wave train. This indicates that the increasing trend of the phase coupling is an important reason for the wave train breaking in shallow water.

Figures 9 and 10 depict the wavelet-based bicoherence spectra for the case of a JONSWAP ($\gamma = 7$) wave train (Test 7) at eight locations along the wave flume. No bispectral peak appears at $b^2(2f_p, f_p)$ and this is may be not surprising as no clear third harmonic $3f_p$ is present in the frequency spectrum (Fig. 4). Furthermore, wavelet-based bicoherence diagrams show that the phase coupling reaches its maximum level at frequencies slightly higher than the exact harmonics ($2f_p$, $3f_p$ ...). This result is consistent with the results of Ma et al., 2010 who explained this process by the slight upshift of peak values in spectrum at higher harmonics, which is readily seen in Fig. 4. The fact that clear 1st, 2nd and 3rd harmonics are not present, is possibly due to other mechanisms such as quadruplet interactions ($f_1+f_2 = f_3+f_4$, Elgar et al., 1995) which have a shape stabilizing impact on the spectrum and are confined to free waves. This result is consistent with the peak frequency downshift demonstrated experimentally in Stansberg, 1994 and Abroug et al., 2020, where it was interpreted as a self-stabilizing feature.

https://doi.org/10.5194/nhess-2020-209
Preprint. Discussion started: 20 July 2020

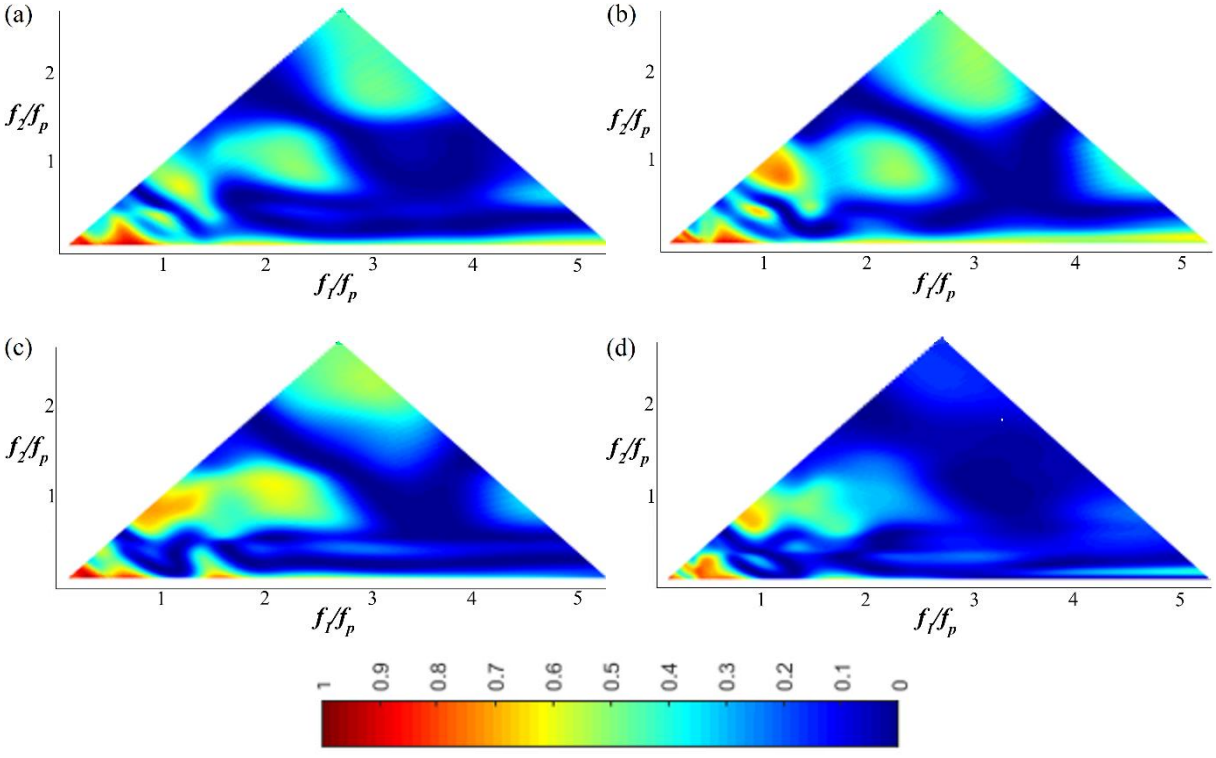

Figure 8: The wavelet-based bicoherence spatial evolution on the sloping bottom for JONSWAP ($\gamma = 3.3$) wave train (Test 5). (a): x = 10.20 m; (b): x = 11.20 m; (c): x = 12.40 m; (d): x = 13.60 m.

Figure 11 summarizes the variability in the location and intensity of the wavelet-based bicoherence between the bifrequency pairs (f_p, f_p), ($2f_p$, f_p), ($3f_p$, f_p), ($4f_p$, f_p), ($2f_p$, $2f_p$) for several tests. The two vertical solid lines and the dotted line respectively indicate the breaking region and the toe of the slope. This figure indicates that the steepness has a strong influence on the non-linear phase coupling between harmonics in intermediate water depth (h_0 = 0.3 m). Non-linear wave-wave interactions and their increasing trend is more important for wave trains having strong non-linearities. Beyond the wave breaking ($x > x_b$), the decreasing trend of the non-linear phase coupling among harmonics is also more significant in the case of strong steepness S_0. This result is in accordance with the dissipation related to breaking, which is particularly noticeable when the wave steepness is high (Abroug et al., 2020).

An important similarity between different spectra, is that important wave-wave interactions are mostly limited to the first harmonics of primary waves (f_p,f_p), ($2f_p$,f_p). This finding is consistent with the energetic behavior of wave trains downstream the wave breaking (Abroug et al., 2020). Moreover, in the case of small and moderate wave steepness (Test 2 and Test 6), the phase coupling varies slightly downstream the wave breaking compared to that found prior the breaking, suggesting that a small energy transfer happens downstream the breaking location.

https://doi.org/10.5194/nhess-2020-209
Preprint. Discussion started: 20 July 2020

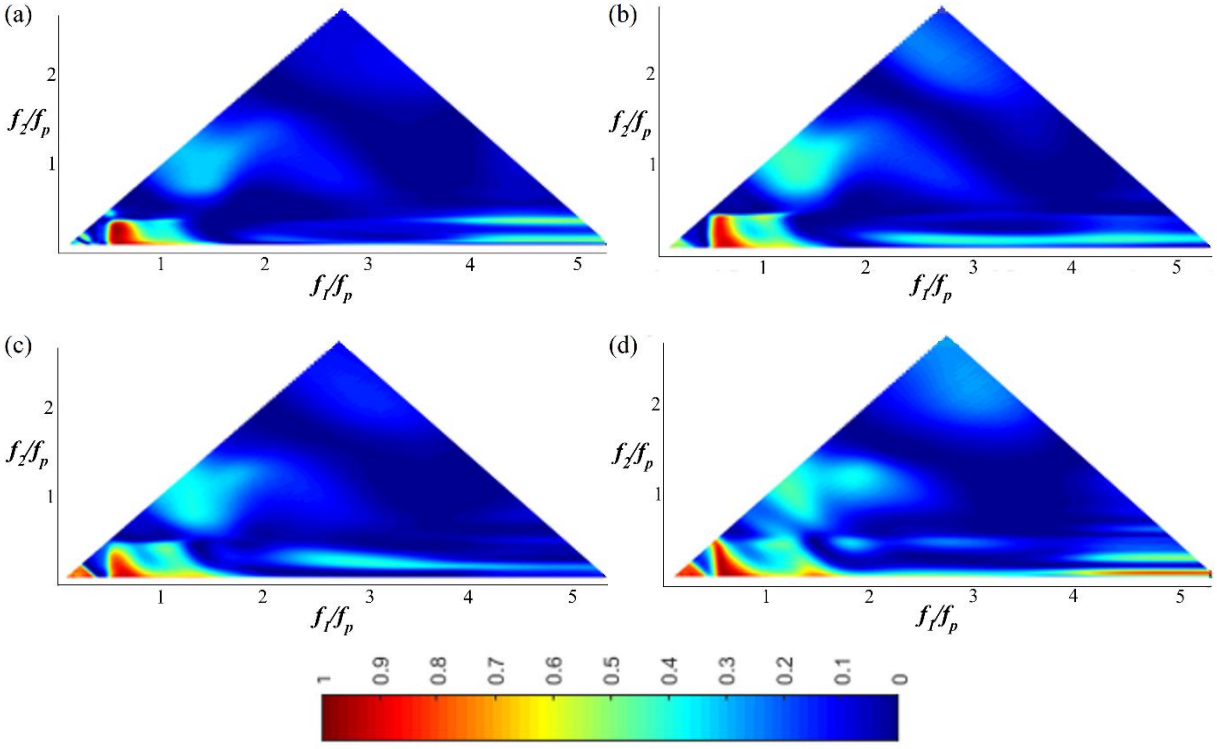

Figure 9: The wavelet-based bicoherence spatial evolution on the flat bottom for JONSWAP (γ = 7) wave train (Test 7). (a): x = 4 m; (b): x = 6.4 m; (c): x = 8 m; (d): x = 9.6 m.

It can be concluded that bound or non-resonant interactions play a crucial role in the propagation process and breaking of wave trains in shallow water depth. Although the bound waves are not supposed to contribute to the energy redistribution, our experimental observations raise the question of the impact of bound interactions on dissipation and energy transfers among different frequency components.

5 Conclusions and perspectives

An experimental approach is proposed for determining the non-linear wave-wave interactions, which accompany the propagation of large amplitude wave trains, that might cause damage to coastal zones, marine structures and navigation vessels. We investigate seven focused wave trains derived from JONSWAP (γ = 3.3 or 7) and Pierson-Moskowitz spectra propagating from intermediate water depth to the inner surf zone. The results presented in this study extend the parameter range of observations of triad interactions. Focusing waves were generated in a physical wave flume by modifying the wave spectrum and steepness. The present data were collected in intermediate water with a $k_p h_0$ varying between 0.92 and 0.79.

https://doi.org/10.5194/nhess-2020-209
Preprint. Discussion started: 20 July 2020

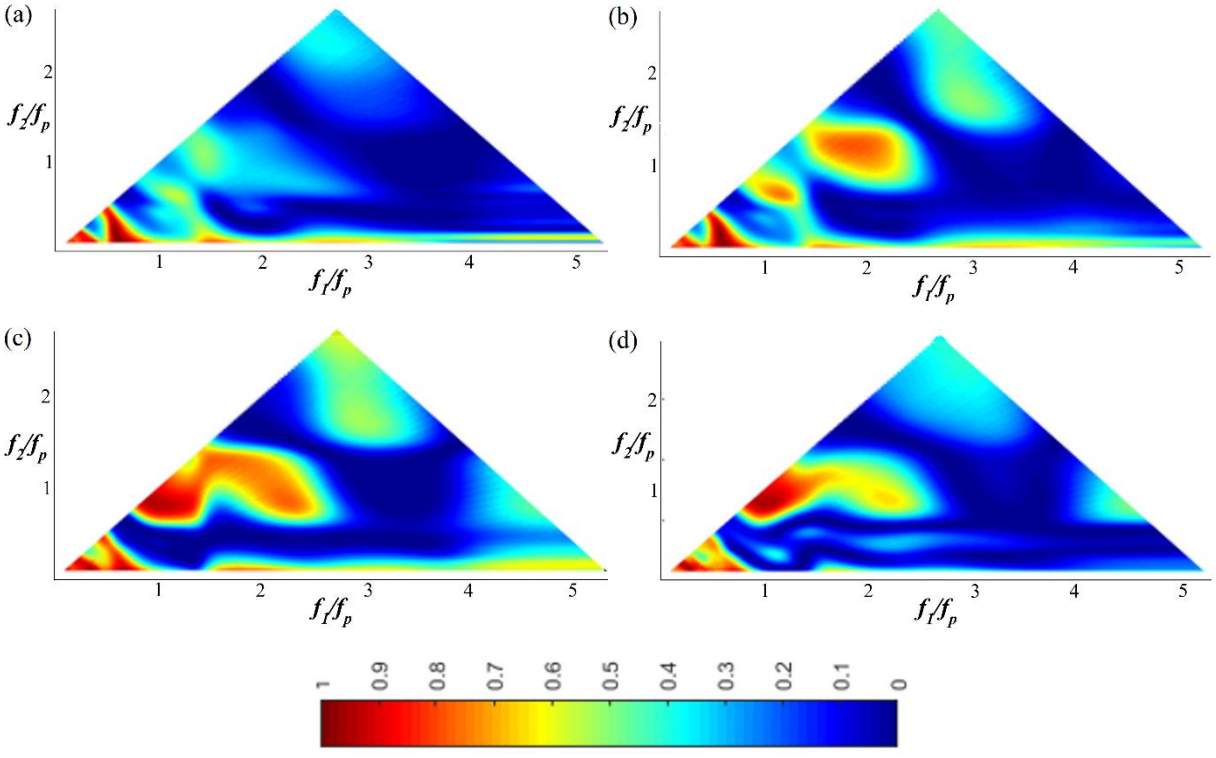

Figure 10: The wavelet-based bicoherence spatial evolution on the sloping bottom for JONSWAP (γ = 7) wave train (Test 7). (a): *x* = 10.2 m; (b): *x* = 11 m; (c): *x* = 12.4 m; (d): *x* = 13.8 m.

A typical wave train consists of a large number of waves interacting with one another. Wavelet-based bicoherence is utilized to investigate the non-linear phase coupling between frequency components of short time series. Some consequences of non-linear transfer are briefly discussed; in particular the role played by non-linear interactions in shaping the high frequency part of the spectrum, the relative contribution of each harmonic and the downshifting of the peak spectrum demonstrated in previous studies.

Along the flat bottom (4 m < *x* < 9.5 m), one might assume that the influence of triad interactions is very weak for the two considered spectra. The bispectral analysis of the data shows that as the waves propagate along the flat bottom, the magnitude of the bicoherence increases slightly (between 0% and 20% of its initial value). Moreover, this is foreseeable because the spectrum and the wave train shape do not substantially change along the flat bottom and a small amount of energy is relocated from the peak region to high frequency wave components. The spectra remain approximately unimodal and do not present a clear second or third harmonic and non-linear interactions concern only the peak and low frequency regions. On the flat bottom, the wave train is still dispersive and consequently, bound interactions are responsible for the slight growth of $b^2(f_p,f_p)$ and $b^2(0.5f_p, 0\text{-}0.5f_p)$.

https://doi.org/10.5194/nhess-2020-209
Preprint. Discussion started: 20 July 2020

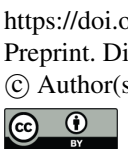

Natural Hazards and Earth System Sciences
Discussions

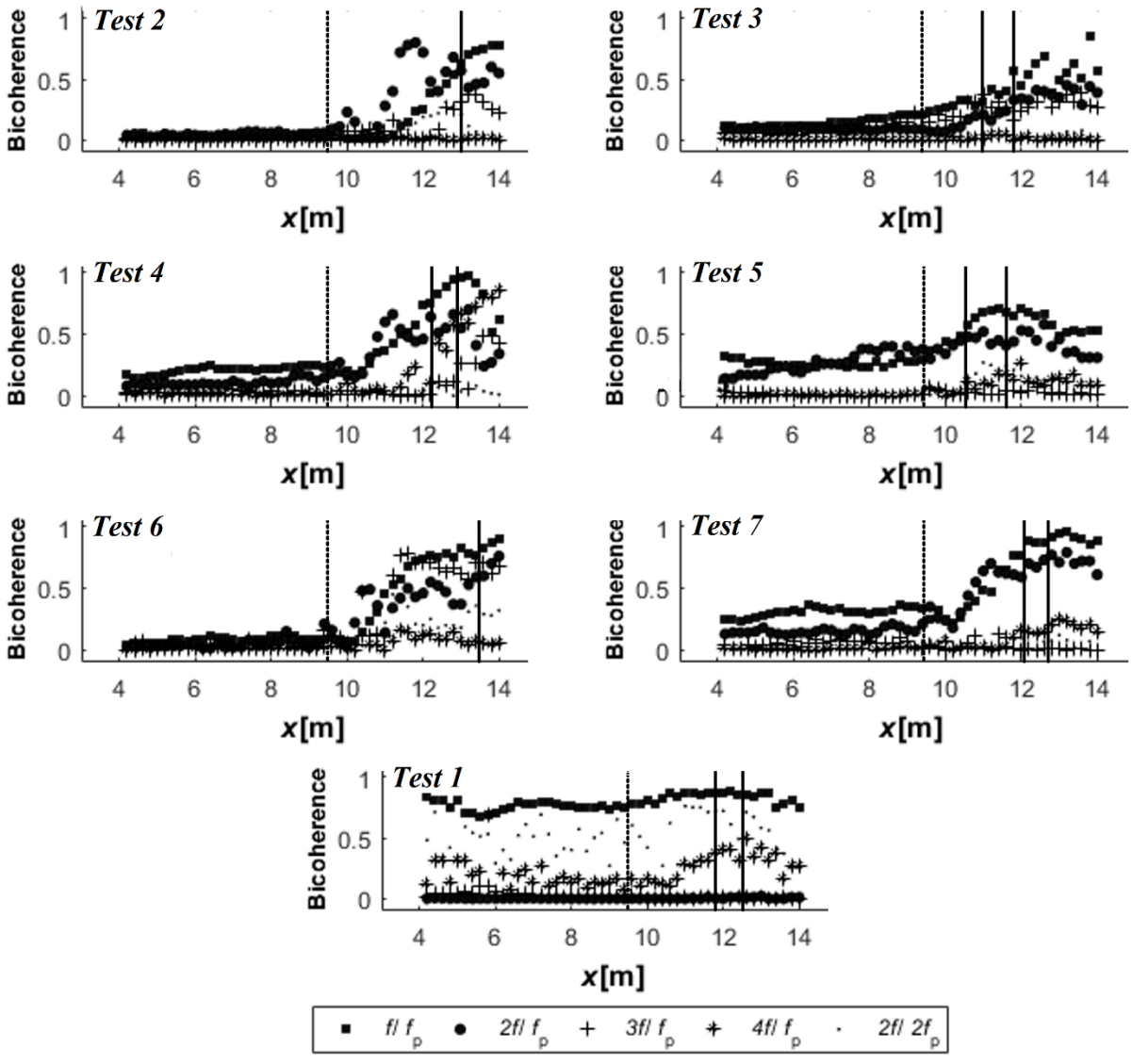

Figure 11: Spatial variation of the wavelet-based bicoherence among harmonics.

When the wave train reaches the slope (9.5 m < x < x_b), wave-wave interactions among high order harmonics increase rapidly and reach the maximum degree in the breaking/focus location. The analysis showed a gradual broadening of the bicoherence spectrum, which is in accordance with previous studies who demonstrated that the energy is transferred mainly to high frequencies regions. This is partly due to significant spectral transformations which are more important during the shoaling process. Particularly, this analysis showed a considerable contribution of 2nd and 3rd harmonics for unidirectional steep wave trains and the spectral components at the second harmonic $2f_p$ have increased substantially (6 times its initial value). The

https://doi.org/10.5194/nhess-2020-209
Preprint. Discussion started: 20 July 2020


Natural Hazards and Earth System Sciences Discussions

bispectral analysis results show that the wave non-linearity S_0 plays an important role in the increasing trend of phase coupling, which is more important for wave trains having strong non-linearities.

The results obtained in this study show important features in wave-wave interactions during the propagation of focused waves. This study strengthens the usefulness of wavelet-based analysis in detecting features that are hidden in a Fourier-based analysis, and in explaining several phenomena, i.e. the process leading to wave breaking and the energy transfer between wave components. Nonetheless, to confirm the use of wavelet-based bicoherence for realistic 3D studies with coastal structures, efforts are needed to expand this study for example by investigating greater water depths, higher steepness and wider spectra. Moreover, the observed spatial evolution of wavelet-based bicoherence for focused wave trains should be compared to that of waves with similar steepness and bandwidth but with random distribution of phase. In other words, efforts should be made to identify and quantify the phase coupling differences between focusing wave trains and non-focusing waves. Finally, a detailed study of how bound energy at harmonics would be influenced by quadruplet interactions should be performed.

Competing interests

The authors declare that they have no conflict of interest.

Acknowledgments

This work has been carried out within the framework of the DYNAT (Dynamique du littoral et risques NATurels) project and has received funding from the Normandy region. We thank L. Perez and D. Mouazé for providing technical supports during the experiments. The authors wish also to express their gratitude to S. Baatout for her thorough re-reading of this article.

References

Abroug, I., Abcha, N., Dutykh, D., Jarno, A and Marin, F.: Experimental and numerical study of the propagation of focused wave groups in the nearshore zone, Phys. Lett. A, 384, 6, 126144, doi:10.1016/j.physleta.2019.126144, 2020.

Abroug, I., Abcha, N., Jarno, A and Marin, F.: Physical modelling of extreme waves: Gaussian wave groups and solitary waves in the nearshore zone, Advances and Applications in Fluid Mechanics, 23, 2, 141–159, doi:10.17654/FM023020141, 2019

Bai, Y., Xia, X., Li, X., Wang, Y., Yang, Y., Liu, Y., Liang, Z and He, J.: Spinal cord stimulation modulates frontal delta and gamma in patients of minimally consciousness state, Neuroscience, 346, 247–254, doi: 10.1016/j.neuroscience.2017.01.036, 2017

Becq-Girard, F., Forget, Ph and Benoit, M.: Nonlinear propagation of unidirectional wave fields over varying topography, Coast. Eng, 38, 2, 91–113, doi:10.1016/S0378-3839(99)00043-5, 1999.

https://doi.org/10.5194/nhess-2020-209
Preprint. Discussion started: 20 July 2020

Didenkulova, I and Anderson, C.: Freak waves of different types in the coastal zone of the Baltic Sea, Nat. Hazard. Earth. Syst. Sci, 10, 2021–2029, doi:10.5194/nhess-10-2021-2010, 2010.

Dong, G., Yuxiang, Ma., Perlin, M., Xiaozhou, M., Bo, Y and Jianwu, X.: Experimental study of wave-wave nonlinear interactions using the wavelet-based bicoherence, Coast. Eng, 55, 9, 741–752, doi:10.1016/j.coastaleng.2008.02.015, 2008.

Dysthe, K., Krogstad, H. E and Müller, P.: Oceanic rogue waves, Annu. Rev. Fluid Mech, 40, 287–310, doi: 10.1146/annurev.fluid.40.111406.102203, 2008.

Eldeberky, Y and Madsen, P. A.: Deterministic and stochastic evolution equations for fully dispersive and weakly nonlinear waves, Coast. Eng, 38, 1, 1–24, doi:10.1016/S0378-3839(99)00021-6, 1999.

Eldeberky, Y.: Nonlinear transformation of wave spectra in the nearshore zone, PhD Thesis, published as Communications on Hydraulic and Geotechnical Engineering, Delft University of Technology, Faculty of Civil Engineering, Report No. 96-4, 203, 1996.

Elgar, S., Herbers, T. H. C., Chandran, V and Guza. R. T.: Higher-order spectral analysis of nonlinear ocean surface gravity wave, J. Geophys. Res, 100, 4983–4997, doi:10.1029/94JC02900, 1995.

Elsayed, M. A. K.: A novel technique in analyzing non-linear wave-wave interaction, Ocean. Eng, 33, 2, 168–180, doi:10.1016/j.oceaneng.2005.04.010, 2006.

Fedele, F., Herterich, J., Tayfun, A and Dias, F.: Large nearshore storm waves off the Irish coast, Scientific Reports 9, 1, 15406, doi:10.1038/s41598-019-51706-8, 2019.

Grinsted, A., Moore, J. C and Jevrejeva, S.: Application of the cross wavelet transform and wavelet coherence to geophysical time series, Nonlinear. Proc. Geoph, 11, 561–566, doi:10.5194/npg-11-561-2004, 2004.

Huseni, GH and Balaji, R.: Wavelet transform based higher order statistical analysis of wind and wave time histories, Journal of the institution of engineers (India), Ser. C , 98, 635–640, doi:10.1007/s40032-016-0287-0, 2016.

Janssen, P. A. E. M and Onorato, M.: The intermediate water depth limit of the Zakharov equation and consequences for wave prediction, J. Phys. Oceanogr, 37, 2389–2400, doi:10.1175/JPO3128.1, 2007.

Kharif, C and Pelinovsky, E.: Physical mechanisms of the rogue wave phenomenon, Eur. J. Mech. B-Fluid, 22, 603–635, doi:10.1016/j.euromechflu.2003.09.002, 2003.

Kharif, C., Pelinovsky, E and Slunyaev, A.: Rogue waves in the ocean, Springer Verlag, berlin Heldelberg, 2009.

Larsen, Y., Hanssen, A and Pecseli, H. L.: Analysis of non-stationary mode coupling be means of wavelet-bicoherence, Int. Conf. Acoust. Spee, 6, IEEE, New York, 3581–3584, doi: 10.1109/ICASSP.2001.940616, 2001.

Li, Y., Wang, X and Lin, J.: Fault diagnosis of rolling element bearing using nonlinear wavelet bicoherence features, IEEE Conference on prognostics and health management (PHM), Cheney, WA, 22–25 June, 1–6, doi: 10.1109/ICPHM.2014.7036369, 2014.

Liang, S., Zhang, Y., Sun, Z and Chang. Y.: Laboratory study on the evolution of waves parameters due to wave breaking in deep water, Wave Motion, 68, 31–42, doi:10.1016/j.wavemoti.2016.08.010, 2017.

https://doi.org/10.5194/nhess-2020-209
Preprint. Discussion started: 20 July 2020

375 Ma, Y., Dong, G., Liu, S., Zang, J., Li, J and Sun, Y.: Laboratory study of unidirectional focusing waves in intermediate depth water, J. Eng. Mech, 136, 1, doi:10.1061/(ASCE)EM.1943-7889.0000076, 2010.

Merkoune, D., Touboul, J., Abcha, N., Mouazé, D., Ezersky, A.: Focusing wave group on a current of finite depth, Nat. Hazard. Earth. Syst, Sci, 13, 2941–2949, doi:10.5194/nhess-13-2941-2013, 2013.

Milligen, B. P. V., Sanchez, E., Estrada, T., Hidalgo, C., Branas, B., Carrersa, B and Garcia, L.: Wavelet bicoherence: a new
380 turbulence analysis tool, Phys. Plasma, 2, 8, 3017–3032, doi:10.1063/1.871199, 1995.

Onorato, M., Residori, S., Bortolozzo, U., Montina, A and Arecchi, F.: Rogue waves and their generating mechanisms in different physical contexts, Phys. Rep, 528, 48–89, doi:10.1016/j.physrep.2013.03.001, 2013.

Stansberg. C. T.: Effects from directionality and spectral bandwidth on nonlinear spatial modulations of deep-water surface gravity wave trains, Coast. Eng, Proceedings of the XXIV international conference, 23–28, Kobe, Japan, 579–593,
385 doi:10.1061/9780784400890.044, 1994.

Tian, Z., Perlin, M and Choi, W.: Frequency spectra evolution of two-dimensional focusing wave groups in finite water depth water, J. Fluid. Mech, 688, 169–194, doi:10.1017/jfm.2011.371, 2011.

Torrence, C and Compo, G. P.: A practical guide to wavelet analysis, Bulletin of American meteorology society, 79, 1, 61–78, doi:10.1175/1520-0477(1998)079<0061:APGTWA>2.0.CO;2, 1998.

390 Vyzikas, T., Stagonas, D., Buldakov, E and Greaves, D.: The evolution of free and bound waves during dispersive focusing in a numerical and physical flume, Coast. Eng, 132, 95–109, doi:10.1016/j.coastaleng.2017.11.003, 2018.

Xu, Guochun., Hao, H., Ma, Q and Gui, Q.: An experimental study of focusing wave generation with improved wave amplitude spectra, Water, 11, 12, 2521, doi:10.3390/w11122521, 2019.

Young, I. R and Eldeberky, Y.: Observations of triad coupling of finite depth wind waves, Coast. Eng, 33, 137–154,
395 doi:10.1016/S0378-3839(98)00006-4, 1998.

Zhang, J., Benoit, M., Kimmoun, O., Chabchoub, A and Hsu, H. C.: Statistics of extreme waves in coastal waters: large-scale experiments and advanced numerical simulations, Fluids, 4, 2, 99, doi:10.3390/fluids4020099, 2019.